University of Glasgow

Robb, P.D. and Craven, A.J. (2008) *Column ratio mapping: a processing technique for atomic resolution high angle annular dark field(HAADF) images.* Ultramicroscopy, 109 (1). pp. 61-69. ISSN 0304-3991

http://eprints.gla.ac.uk/6530/

Deposited on: 24 July 2009

Enlighten – Research publications by members of the University of Glasgow
http://eprints.gla.ac.uk

Column ratio mapping: a processing technique for atomic resolution high angle annular dark field (HAADF) images

Paul D. Robb[1,2*], Alan J. Craven[1,2]

[1]Department of Physics & Astronomy, University of Glasgow, G12 8QQ, UK

[2]SuperSTEM Laboratory, Daresbury Laboratory, WA4 4AD, UK

**Correspondence:* Room 110
Department of Materials
Imperial College London
Exhibition Road
London SW7 2AZ
p.robb@imperial.ac.uk

Abstract

An image processing technique is presented for atomic resolution high angle annular dark field (HAADF) images that have been acquired using scanning transmission electron microscopy (STEM). This technique is termed column ratio mapping and involves the automated process of measuring atomic column intensity ratios in high-resolution HAADF images. This technique was developed to provide a fuller analysis of HAADF images than the usual method of drawing single intensity line profiles across a few areas of interest. For instance, column ratio mapping reveals the compositional distribution across the whole HAADF image and allows a statistical analysis and an estimation of errors. This has proven to be a very valuable technique as it can provide a more detailed assessment of the sharpness of interfacial structures from HAADF images. The technique of column ratio mapping is described in terms of a [110]-oriented zinc-blende structured AlAs / GaAs superlattice using the 1Å-scale resolution capability of the aberration-corrected SuperSTEM 1 instrument.

PACS codes: 68.37.-d; 68.37.Ma

Keywords: High angle annular dark field (HAADF) imaging; column ratio mapping; image processing

1. Introduction

In recent years, the performance of electron microscopes has been greatly improved through the implementation of practical aberration correction technology [1-3]. This has allowed the creation of instruments that can form 1Å-scale electron probes at accelerating voltages of only 100kV [5,6]. As an example, SuperSTEM 1 was the first UK based aberration-corrected 100kV FEG-STEM (field emission gun-scanning transmission electron microscope) that was capable of achieving a spatial resolution of 1Å.

Instruments, such as SuperSTEM 1, are now capable of resolving the smallest atomic plane spacing along the [001] crystal growth direction in the economically important III-V compound semiconductors [7]. For instance, the 1.4Å dumbbell spacing between Ga and As atomic planes along the [001] direction in GaAs (a zinc-blend structure) can be easily resolved in high angle annular dark field (HAADF) images from SuperSTEM 1. Such images are commonly referred to as atomic number (Z) contrast images since the recorded image intensity varies approximately with the square of the atomic number of the atomic columns present in the specimen due to Rutherford-like scattering [8-12]. Hence, columns with different mean Z^2 can be readily distinguished. It has also been widely reported that the HAADF imaging technique can provide atomic resolution structure images that are generally easier to interpret than conventional high-resolution conventional transmission electron microscope images [8-12]. This is due to the fact that no contrast reversals are observed in HAADF images over a wide range of spatial frequencies. Hence, SuperSTEM 1 HAADF images provide the opportunity to investigate the compositional distribution of semiconductors on a scale of individual atomic layers and, therefore, allow a precise evaluation of the associated growth techniques.

Despite the obvious benefits of aberration-corrected STEM, experience with SuperSTEM 1 has revealed the necessity of applying image analysis techniques in order to take full advantage of the unprecedented spatial resolution. For instance, it is very difficult to determine the precise compositional distribution of a sample by simply looking at a high-resolution HAADF image. The usual method of investigation involves the intricate process of drawing several intensity line profiles across one part of the image, which must then be analysed individually. In the case of [001] grown III-V semiconductors viewed along the <110> direction, the important quality of interfacial sharpness is often evaluated by

examining the change in the ratio of the Group III and Group V column intensities in each dumbbell across layer boundaries. In this approach, the level of sharpness is given by the distance over which the column ratio switches in value across the boundary [13-17]. This distance is called the transition region of the boundary.

However, the usual approach is often problematical and unsatisfactory for a number of reasons. First of all, the measurement of the intensity ratio is liable to human error if particular care is not taken. Part of the problem is that subjective interpretation of dumbbell intensity profiles can occur if there is no exact criteria to measure the dumbbell column ratio or if the method is not consistently applied to every dumbbell intensity profile. Consequently, it is difficult to properly quantify the interfacial sharpness and the eventual value that is reported may be incorrect. Furthermore, no estimation of the error in the column ratio value is provided by the usual approach. An additional difficulty concerns the existence of an underlying background image signal. For instance, following the simple qualitative model of image contrast of Klenov and Stemmer, high spatial resolution information in HAADF images is associated with column intensities that sit on top of a background signal [18]. The background signal is generated from the average scattering from the material sampled by the de-channelled probe and, therefore, gives non-local information about the specimen. Hence, in order to associate the change in the column intensity ratio with the change in local composition, the underlying background signal must be removed before the column ratio is measured [18-23]. However, it is not a straight forward matter to separate the background signal from the high-resolution column intensities especially across interfaces where the background changes in value. This adds a further complication to the measurement of the column ratio. Finally, the usual approach frequently neglects a great deal of the information contained within the image because only a few selected line profiles are analysed in detail. This can often lead to an erroneous estimation of the interfacial sharpness if the area chosen for analysis is not representative of the entire interface.

In order to overcome the problems outlined above, this paper will demonstrate a processing technique (called column ratio mapping) that has been successfully used to analyse high-resolution SuperSTEM 1 HAADF images. This technique is described using a high-magnification SuperSTEM 1 HAADF image of an AlAs / GaAs superlattice that was grown by molecular beam epitaxy (MBE) [17]. Column ratio mapping involves the conversion of a standard HAADF image into a map that displays the column ratio value for every dumbbell

position in the original image. The column ratio for every dumbbell is measured in a consistent fashion using an automated procedure that is carried out by computer programs written in the DigitalMicrograph^{TM} (Gatan Inc.) scripting language. Moreover, the column ratio is measured in the absence of the background signal. Hence, the technique makes it possible to actually see the distribution of the dumbbell shapes and, therefore, the local compositional variation in an image at a glance. This greatly improves the analysis of specimens by providing a fuller picture of the elemental distribution across the entire image which is also free from human error. In addition, column ratio mapping also permits a statistical analysis of the distribution of the dumbbell column ratio values to be carried out. The column ratio technique then leads to a more accurate estimation of the overall interfacial sharpness as described below.

2. Theory

2.1 Instrumentation

The high-resolution HAADF image that is analysed in this paper was obtained from SuperSTEM 1. This instrument is a VG HB501 100kV STEM that has been retrofitted with a second generation NION aberration corrector [5,6]. The microscope contains a cold FEG that is operated with an extraction voltage below 4kV. The energy spread from the gun is 0.3eV and has a gun brightness of about 10^9Acm^{-2}Sr^{-1}. The microscope is equipped with a scintillator-photomultiplier tube based HAADF detector and a Gatan-ENFINA spectrometer (energy resolution ~0.35eV). In this mode of operation, the HAADF detector has inner and outer angles of 70mrad and 210mrad, respectively. The HAADF image was acquired using a probe semi-convergence angle of 24mrad and the image black level was set so that a few image counts (~5-10) were recorded in the absence of the specimen. Typical image counts are of the order of several thousand in the presence of the specimen. Furthermore, a specimen drift rate of much less than 5nm per hour can be achieved in SuperSTEM 1. This is considerably better than the drift rate in most commercial microscopes. Finally, the superlattice specimen was prepared using the cross-section technique and was finished with a low energy ion mill at 400eV and at an angle of 6° using a Technoorg Linda GentleMill [25].

2.2 The dumbbell column ratio of AlAs / GaAs layers

The AlAs / GaAs system is typically grown on top of a GaAs substrate along the [001] crystal direction by techniques such as MBE [7,17]. When using STEM to study interfaces in this system, the normal practice is make a cross-section specimen and look down a <110> direction (here [110]) because atomic spacings are generally larger compared to other zone-axis orientations and because interfacial steps along the $[1\bar{1}0]$ direction can be seen edge on [19]. Crystal directions are specified with respect to the primary wafer flat and this is defined by the manufacturers as being the [110] direction.

The projection along the [110] orientation in the AlAs / GaAs system forms the familiar dumbbell configuration that is characteristic of zinc-blende materials. In this way, every single dumbbell is constructed from two atomic columns- a column made up of Group III atoms and a column made up of Group V atoms and these columns are separated by the (004) plane spacing. The AlAs / GaAs superlattice studied in this paper was grown by MBE with As (Z=33) being the only Group V element present and, therefore, every Group V column is made up entirely of As atoms. In comparison, the Group III column of a dumbbell can be populated by two different types of Group III atoms i.e. Al (Z=13) or Ga (Z=31). Thus, the transition from one layer to the next is manifested by a change in the composition of the Group III column in a dumbbell. For example, the Group III column of a dumbbell that is situated in the transition region at an AlAs / GaAs interface would be partly composed of Al and Ga atoms rather than all Al or all Ga atoms. The transition region can be a result of either elemental diffusion or the presence of surface steps along the interface [26,27].

Due to the Z-contrast nature of HAADF images, a HAADF intensity profile of a dumbbell can be used to estimate the average composition of the Group III column relative to the As column. One way of quantifying a dumbbell intensity profile is through the calculation of the dumbbell column ratio. This ratio is equal to the Group III column HAADF intensity divided by the As column HAADF intensity. The column HAADF intensity is defined as the maximum HAADF intensity located at a particular column position (I_{Ga} or I_{As} for a GaAs dumbbell) minus the underlying background signal (I_{BD}). As an example, the column ratio of a GaAs dumbbell is given by:

$$\frac{\text{Ga column HAADF intensity}}{\text{As column HAADF intensity}} = \frac{I_{Ga} - I_{BD}}{I_{As} - I_{BD}}$$

Whereas the column HAADF intensity (to a first approximation) is a result of the scattering associated with the channelling of the probe down an individual atomic column, I_{BD} is a result of the average scattering from many different columns due to probe spreading [18,24]. Fig. 1 gives an example of a SuperSTEM 1 HAADF intensity profile of 3 GaAs dumbbells. Every point of the intensity profile was generated from the average of 10 image pixels summed along the $[1\bar{1}0]$ direction. Every intensity profile presented in this paper was generated in the same fashion. It is apparent from Fig. 1 that the Ga and As column intensities sit on top of a uniform background level. The column ratio is equal to 0.96 for the middle dumbbell shown in Fig. 1.

For the superlattice presented in this paper, the column ratio is always defined with reference to the As column intensity. Hence, the column ratio will typically have a value less than 1 for dumbbells that contain a Group III column composed of atoms with a smaller average scattering power than that of As (e.g. an AlAs dumbbell). However, when the scattering power of the Group III column is greater than that of As, the column ratio will typically have a value greater than 1. For example, the In ($Z = 49$) column of an InAs dumbbell is more intense than the As column in this simple approach. In this way, the value of the column ratio provides an estimate of the composition of the Group III column of a particular dumbbell. However, it should be noted that the Z^2 dependence of HAADF imaging is an oversimplification since the HAADF intensity is influenced by many factors. These factors include the microscope accelerating voltage, the detector angles and the defocus value [18]. In addition, the structure and composition of the atomic columns of the specimen also influence the column ratio as does the specimen thickness [18-24]. Hence, it is not always possible to definitively state the Group III column composition from a single value of the column ratio. Nevertheless, in most cases, this is not usually a problem since it is only the change in the column ratio across an interface that is important as it is this that identifies the spatial extent of the transition region and, hence, the interfacial sharpness. A subsequent paper will detail the measurement of the variation in the column ratio for AlAs and GaAs as a function of specimen thickness.

3. Image processing technique

3.1 Background signal removal

Fig. 2(a) is a HAADF image of a [110]-oriented superlattice with a repeat unit consisting of 9ML AlAs / 9ML GaAs. 1ML of a composite material (such as GaAs) is defined as containing 2 atomic planes each made from a different type of atoms. Hence, 1ML of this sort of material appears as a single row of dumbbells perpendicular to the [001] direction in Fig. 2. In addition, the layers were grown epitaxially on top of a GaAs substrate along the [001] crystal direction by MBE with an intended sharpness of 1ML. The local specimen thickness is 40nm. The conversion of the image in Fig. 2(a) into a column ratio map will now be used to describe the column ratio mapping technique.

As mentioned previously, in order to leave only the high spatial resolution column intensities, an image (such as in Fig. 2(a)) must have the background signal removed. When confronted with an image of a material with uniform composition (and constant thickness) across the image dimensions then it is a simple manner to subtract the background as it manifests itself as a uniform intensity level. However, a modulated background signal is obtained from an image of an interface because the average composition changes across the dimensions of the image. Hence, the background cannot simply be subtracted and some additional steps are required.

The first step in the background removal process involves the application of a circular mask on the Fourier transform (FT) of the image through the use of the DigitalMicrograph software package. The mask removes the low spatial frequencies that give rise to the modulated background (e.g. superlattice reflections in the case of the superlattice) [28]. Fig. 3 shows the FT of the image of the 9ML AlAs / 9ML GaAs superlattice. Fig. 3 also illustrates the size of mask that is typically used. The process of background removal works best if the mask is smoothed by 5 pixels otherwise unwanted artefacts can arise. In addition, the size of mask should be large enough to eliminate all of the superlattice reflections but not so large that any lattice reflections are entirely or partly removed. For instance, if lattice reflections are clipped then some high spatial resolution information is lost and the processing technique creates a processed image that has incorrect dumbbell profiles and intensities. Fortunately, this is never really a serious problem with III-V materials as all of the low spatial frequencies are confined in close proximity to the central FT spot. Therefore, it is relatively easy to place the mask around these reflections without ever clipping the higher order reflections. In addition, as long as the low spatial frequencies are removed and the high order ones are not clipped, then the circular mask can be of any size and the subsequent steps of the conversion technique will

generate the same column intensity profiles. For example, the final processed image will not be affected if the size of the mask is increased from the smaller mask to the larger one shown in Fig. 3. The larger mask is the limit after which high order reflections start to be clipped.

It should be noted that the mask also removes the central FT spot. Hence, after the masked FT undergoes an inverse FT, a processed image is generated with an average intensity equal to zero in conjunction with no background modulation. In actual fact, in such a processed image, the dumbbell columns have a positive intensity value above zero and the positions between dumbbells have a negative intensity value. The next step of the process then involves the addition of a uniform level of intensity (equal in magnitude to the minimum intensity value in the processed image) across the entire image so that the minimum level in the new processed image is set to zero. This, however, leaves the dumbbell intensities sitting on top of the lowest point of the noise. This small residual background signal (usually about 1-2% of the maximum dumbbell intensity) is taken care of in a later stage of the process. If the small residual background is disregarded for the moment then the addition of the uniform level of intensity gives the desired processed image since the dumbbell columns sit upon a uniformly zero background level.

The background-removed image of the superlattice is shown in Fig. 2(b). It is apparent that the background modulation has been successfully removed. In comparison, Fig. 2(c) only shows the background signal. This was generated by taking the inverse FT of the masked central area only. The same background-removed image is obtained if the background image (Fig. 2(c)) is subtracted from the original image followed by the addition of the uniform level of intensity.

Fig. 4(a) shows an intensity profile taken across a line of dumbbells in the unprocessed image of the 9ML AlAs / 9ML GaAs superlattice (the image that is presented in Fig. 2(a)). In contrast, Fig. 4(b) shows an intensity profile taken across the image in Fig. 2(b) after the removal of the background signal. It is clear that not only has the background modulation from the superlattice been removed but also that the intensity between dumbbells is now zero to within the effect of the noise. It can also be seen that the shape of the unprocessed intensity profile in Figure 4(a) has been preserved in the processed image intensity profile in Figure 4(b). Given the uncertainty in the background subtraction, the column ratios of 0.73 and 0.74 in the unprocessed and processed intensity profiles are in excellent agreement. As was stated

previously, it is this ratio that is of significance in the determination of composition from HAADF images. Therefore, it is apparent that the process of background removal does not introduce any unwanted artefacts into the analysis of composition.

3.2. The measurement of the column ratio for every dumbbell in the background-removed image

The next step in the image conversion process concerns the measurement of the column ratio of every dumbbell in the background-removed image. To begin with, the positions of the all the dumbbells are measured and recorded using DigitalMicrograph's particle locator tool. This tool outputs the image coordinates of the centre of every small area that has intensity above a user-defined threshold value. In order to equate the positions of the small areas with the positions of the dumbbells, the threshold intensity value is set to above zero in the background-removed image. The remainder of the conversion process is carried out through a series of DigitalMicrograph scripts. The following procedure is directly relevant to [110]-oriented zinc-blende specimens but it would be straight forward to adapt it to any system of atomic columns.

To measure the column ratio of the dumbbells, small individual line profiles (40 pixels long and averaged over a width of 10 pixels along the $[1\bar{1}0]$ direction) are drawn across every dumbbell in the background-removed image. In the case of the image in Fig. 2(a), a single pixel has a length equal to 0.0146nm. The middle of each line profile corresponds to the centre of the dumbbell (found from the particle locator tool) and the line profile is long enough to encompass the point half way between the dumbbell and the next one on either side. The elimination of the residual background from a particular line profile is achieved by finding the minimum intensity value (averaged over 3 profile points) on the right hand side (RHS) and left hand side (LHS) of the profile. The average of these two values is then subtracted from the profile. An example of such a dumbbell intensity line profile (taken from the background-removed image of the 9ML AlAs / 9ML GaAs superlattice) is presented in Fig. 5.

Since the column ratio is defined with respect to the As intensity, the side of the dumbbell that contains the As column must be known beforehand. The position of the As can be determined by considering the direction of growth in the image (along [001] in Fig. 2(a)) and

the way in which the specimen was cut from the parent wafer. In the case of the 9ML AlAs / 9ML GaAs superlattice image in Fig. 2(a), the As will is situated in the RHS of each dumbbell.

The line profile of every dumbbell then undergoes the following process one at a time. The position of the peak HAADF intensity on the side of the dumbbell that contains the As column is firstly located. This point is denoted by P_{As}. The HAADF intensity, centred on the point P_{As}, is then averaged over a 3 point wide RHS window to give some averaging of noise (see Fig. 5). This window is shifted across 3 points in order to find the highest average intensity. This gives a measure of the intensity of the As column ($I_{As} – I_{BD}$). The script then finds the position of maximum intensity in an outer LHS window (width equal to 7 points) that is displaced from P_{As} by 10 points to the left. This position is denoted by P_C. The displacement of 10 points was chosen as this is equal to a distance of 1.4Å, which is the dumbbell spacing in GaAs. The script then calculates the average intensity over a LHS inner window that has a width of 3 points and is centred on P_C. The window is slid over 3 different positions to find the highest average intensity. This gives the non-As column intensity ($I_C – I_{BD}$). The ratio is finally calculated by dividing ($I_C – I_{BD}$) by ($I_{As} – I_{BD}$).

The process outlined above was used to measure the column ratio for a large number of dumbbells. The values that were obtained from this automated method were compared with those obtained from the standard approach. It was found that both methods gave very similar results thereby validating the automated approach. Nonetheless, if the magnification changes across an image due to (for example) mains interference, the automated approach would produce an incorrect measure of the column ratio at some locations. However, the degree of magnification change across a standard high-magnification SuperSTEM 1 image is far too low for it to affect the automated approach. For instance, the size of each dumbbell in a SuperSTEM 1 image is always the same across the entire image. Furthermore, in the rare case in which mains interference does affect the size of the dumbbells (e.g. at very high magnifications that are not typically used) this is usually very easy to spot. Another problem that could affect the automated approach is related to specimen drift. However, in SuperSTEM 1, the drift rate is far too low to have a noticeable affect on the calculation of the column ratios.

The error in a single measurement of the dumbbell column ratio was also estimated to be of the order of 5-6%. This error was calculated by considering the standard error of each column intensity measurement. For instance, the intensity of one column is generated from the average intensity of 3 pixels by 10 pixels in the background-removed image. Hence, a standard deviation value can be worked out from the variation in the 30 pixel values that are averaged together to give each column intensity. In this way, a standard error in the column ratio can also be calculated for each dumbbell. It was found that an individual column ratio measurement had an overall standard error of 5-6%. This level of error was consistently observed for many individual dumbbells.

3.3. Column ratio maps

After the column ratio of every dumbbell in the background-removed image is measured, the image is re-plotted as a map containing these values. For instance, every pixel that formed the area of a dumbbell in the image now possesses the associated column ratio value. In this way, the brightest looking dumbbells in the map have the highest ratios. A high column ratio suggests the presence of a powerful scatterer and, hence, the presence of high Z atoms in the non-As column of a particular dumbbell. In addition, the values of the pixels between dumbbells in the map are set to zero.

Fig. 2(d) presents the column ratio map that was calculated from the image of the 9ML AlAs / 9ML GaAs superlattice. The brightest dumbbells are most GaAs-like and the darkest dumbbells are most AlAs-like. The column ratio values range from 0.17 to 1.34 in the map. In contrast to the original image in Fig. 2(a), the column ratio map reveals the distribution of dumbbell shapes at a glance. It is true that a general idea of the superlattice composition can be obtained from looking at the original image in Fig. 2(a). However, this is a result of the background signal that gives only delocalised information (see Fig. 2(c)). On the other hand, the column ratio map provides an assessment of the local composition as it uses the high-spatial information of the column intensities.

Fig. 2(d) illustrates that the overall compositional difference between the 2 types of layers is visible in the map due to the fact that GaAs-like dumbbells are mainly located within the 9ML GaAs repeats and AlAs-like dumbbells are mainly located within the 9ML AlAs repeats. However, the column ratio map also demonstrates that the particular layers do not

have a homogeneous composition as there is some variation within the individual layers. In fact, there does not appear to be a sharp changeover in the column ratio across most of the interfaces. This suggests an overall level of interfacial roughness and non-uniformity that would have been difficult to expose through the use of the usual approach. A more in-depth analysis of the column ratio map is given below.

Column ratio maps can also be visually manipulated in different ways in order to help with extracting useful information from them and also for presentation purposes. For instance, Fig. 6 shows a version of the column ratio map in Fig. 2(d) that has been re-plotted with the dumbbells extended along the [001] direction to fill the gaps between them. This means that an ideal interface is stepped by one dumbbell along the $[1\bar{1}0]$ direction in this view. The variation in the column ratio values across the map may be easier to visualise in this particular version of the column ratio map. The DigitalMicrograph software package also allows other ways of displaying the data including a contour map with a custom colour display (not shown). Thus a variety of display presentations are possible for column ratio maps that allow different features to be highlighted.

4. Analysis of column ratio maps

It is extremely useful to draw line profiles across column ratio maps in order to assess the level of interfacial sharpness. For example, Fig. 7 is an averaged column ratio line profile taken across the column ratio map in Fig. 6. The line profile was generated from the average column ratio of 10 dumbbells summed along the $[1\bar{1}0]$ direction. The error bars in Fig. 7 are equal to the standard error from the 10 average values.

Fig. 7 shows that the column ratio levels out to a value of about 1 in the middle of the GaAs layers (within a 5-6% error of the earlier 0.96 value of GaAs) and levels out to a value of about 0.4 in the middle of the AlAs layers. These values likely correspond to non-As column compositions of 100% Ga and 100% Al, respectively. However, Fig. 7 also reveals the existence of a transition region along each layer boundary. These transition regions contain column ratio values that are intermediate between that of fully GaAs-like and fully AlAs-like. Hence, the width of each transition region provides a measure of the sharpness associated with a particular interface in the superlattice. Furthermore, both interfaces in Fig. 7 have a

transition region width of 3MLs and, therefore, each superlattice interface can be said to compositionally sharp only over this distance. Here a note of caution is required as the depth over which the electron channelling on the atom columns is scattered away in Ga and As columns is less than the specimen thickness whilst it is greater for Al columns. This will be addressed in subsequent publications.

The technique of column ratio mapping also provides the opportunity to perform a statistical analysis of the dumbbell column ratios in order to improve the investigation of composition. To begin with, the mean and standard deviation of the column ratio in the AlAs and GaAs layers can easily be ascertained from the column ratio map of the 9ML AlAs / 9ML GaAs superlattice. In this case, the column ratio mean value of the AlAs and GaAs layers is equal to 0.413 and 0.979, respectively. On the other hand, the column ratio standard deviation of the AlAs and GaAs layers is equal to 0.091 and 0.095, respectively.

The mean and standard deviation values of the different layers can be used to work out how far apart each individual dumbbell column ratio value is from the appropriate mean value. For instance, Fig. 8 illustrates the column ratio map of Fig. 2(d) re-plotted as a standard deviation departure map. In this map, each dumbbell has a value that corresponds to the number of standard deviations that the dumbbell's column ratio value departs from the appropriate mean value. For example, a value of 3 would indicate that a particular dumbbell had a column ratio value that lies within 3 standard deviations of the appropriate mean. Since there are two distinct mean values (e.g. one for the AlAs and GaAs), the dumbbells that make up each layer was considered independently. Thus, dumbbells within the GaAs layers were analysed with respect to the GaAs mean. In the same way, dumbbells within the AlAs layers were analysed with respect to the AlAs mean. Moreover, interfacial dumbbells were analysed with respect to the mean that was closest to the dumbbell's column ratio value.

Fig. 8 is scaled between 0 and 4 with the brightest looking dumbbells having the largest departure away from the mean value (i.e. equal to 4 standard deviations). It is clear from Fig. 8 that the majority of the brightest dumbbells exist along the interfaces between the different layers. This is not surprising due to the effect that interfacial roughness has on column ratio values along layer boundaries. In fact, it is apparent that the interfacial roughness extends over several monolayers along some of the interfaces in Fig. 8. Nevertheless, Fig. 8 also reveals that some interfacial dumbbells do not have a large departure from the appropriate

mean value. This is an indication that some parts of the interfaces are atomically abrupt. Furthermore, the standard deviation departure map demonstrates that the column ratio value is not uniform within the individual layers.

A greater awareness of the distribution of interfacial dumbbells can also be gained through the selection of dumbbells that have a particular range of column ratio values. In order to achieve this, a histogram of the column ratio values is required. A histogram of the column ratio values in the 9ML AlAs / 9ML GaAs superlattice map is given in Fig. 9(a). In this example, there are a total of 1920 different dumbbells. The histogram reveals the presence of two peaks that correspond to the column ratio mean value of the AlAs and GaAs layers, respectively. Dumbbells that have column ratio values intermediate between that of AlAs and GaAs lie between the two peaks in the histogram. This can be seen by comparing the histogram peaks with the two Gaussian plots that give the expected AlAs and GaAs distributions (i.e. calculated from the AlAs and GaAs mean values). For instance, the intermediate values produce a broadening along one side of each histogram peak. These dumbbells are, therefore, considered to be interfacial dumbbells. Hence, by selecting a certain range of dumbbells in the histogram, the positions of these interfacial dumbbells can be highlighted in the associated column ratio map. The dumbbells that lie within the selected range can be seen in Fig. 9(b). Again, it is apparent from Fig. 9(b) that there is a sharp changeover along some of the interfaces at the positions highlighted in Fig. 8. However, it is also clear that some of the interfaces are much less well defined with the presence of many interfacial dumbbells in some areas. Hence, this way of picking out interfacial dumbbells gives an indicator of the overall quality of the interfaces present within a HAADF image.

5. Conclusions

In order to enhance the analysis of HAADF data obtained from the new class of 1Å-scale aberration-corrected instruments, the image processing technique of column ratio mapping has been developed. This partially automated technique provides a more accurate and comprehensive evaluation of the information contained in HAADF images than is usually obtained through the use of the usual methods of analysis. For instance, one of the benefits of column ratio mapping is that it provides an objective and consistent measurement of the column ratio of all of the dumbbells in an image. This measurement takes into consideration only the high-spatial resolution information contained with an image. Furthermore, since no

dumbbell is overlooked using this technique, an improved overall picture of a specimen's composition is revealed. Ultimately, this results in a better evaluation of any interfaces present in the original image.

Although the details of column ratio mapping have been presented with respect to the SuperSTEM 1 image format, it is a straight forward matter to adapt the DigitalMicrograph scripts to deal with the image formats associated with other aberration-corrected instruments. The main difference would concern the way in which the automated procedure measures the column ratio. For example, the number of image pixels that are averaged together to produce the intensity of a single column would have to be altered to suit other image formats. In addition, the column ratio mapping technique could also be modified in order to analyse other crystal orientations of III-V materials (e.g. the <100> orientation) and possibly different types of materials. These materials would have to have a suitable structure consisting of atomic columns in order for the column ratio mapping technique to be applied.

In summary, it is evident that the conversion of an atomic resolution HAADF image into a column ratio map provides a powerful and more complete analysis of a specimen than is possible from the usual approach. Column ratio mapping permits a statistical analysis of interfaces to be performed that highlights local interfacial sharpness, across the entire image, at a glance. This is in conjunction with more accurate measuring of the dumbbell column ratios and an estimation of errors.

Figures

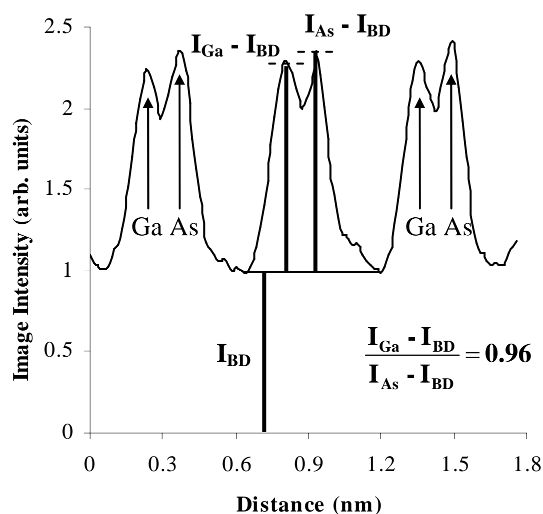

Fig. 1. HAADF intensity profile of 3 GaAs dumbbells along the [001] direction. Every point of the intensity profile was generated from the average of 10 image pixels summed along the $[1\bar{1}0]$ direction. I_{Ga} and I_{As} refer to the peak HAADF intensity on the Ga and As columns of the middle dumbbell. I_{BD} refers to the background intensity. The value of the dumbbell column ratio is also given.

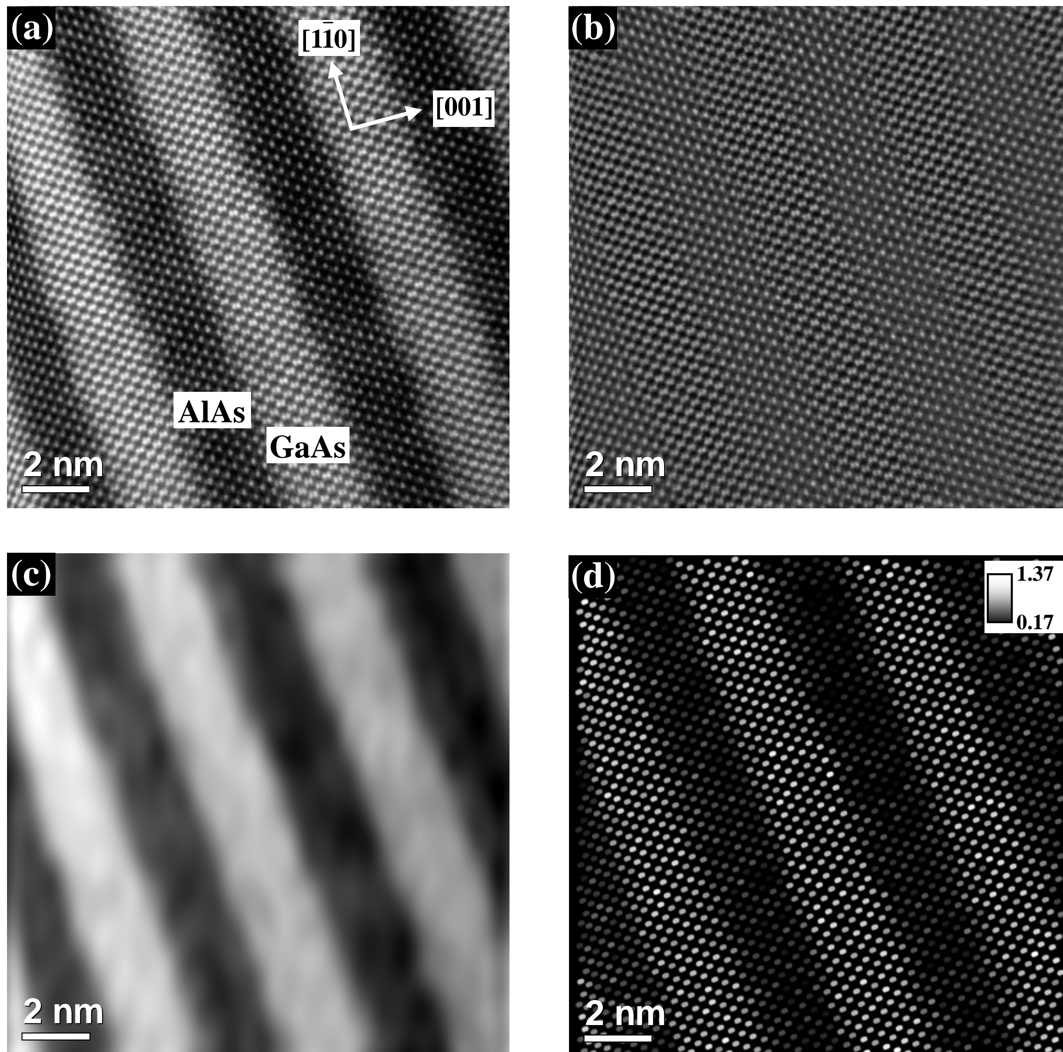

Fig. 2. (a) HAADF image of several repeats of a 9ML AlAs / 9ML GaAs superlattice. The GaAs layers appear as the most intense due to the properties of the underlying background signal. (b) The background removed image of (a). (c) The underlying background signal of the original image in (a). (d) The dumbbell column ratio map. Bright dumbbells have high column ratios and are more GaAs-like. Dark dumbbells have low column ratios and are more AlAs-like.

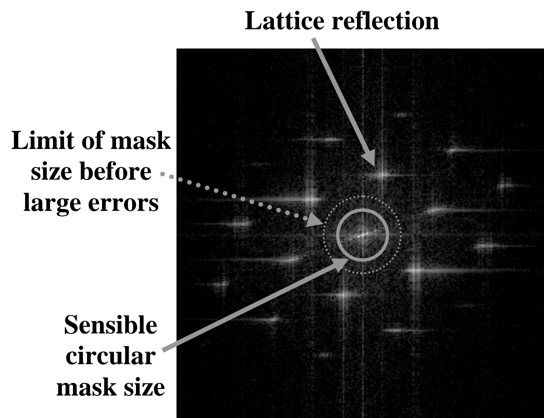

Fig. 3. Fourier transform of the image of the 9ML AlAs / 9ML GaAs superlattice. Two different mask sizes are shown around the central FT spot. The largest mask shows the limit in the size of the mask before lattice reflections are clipped.

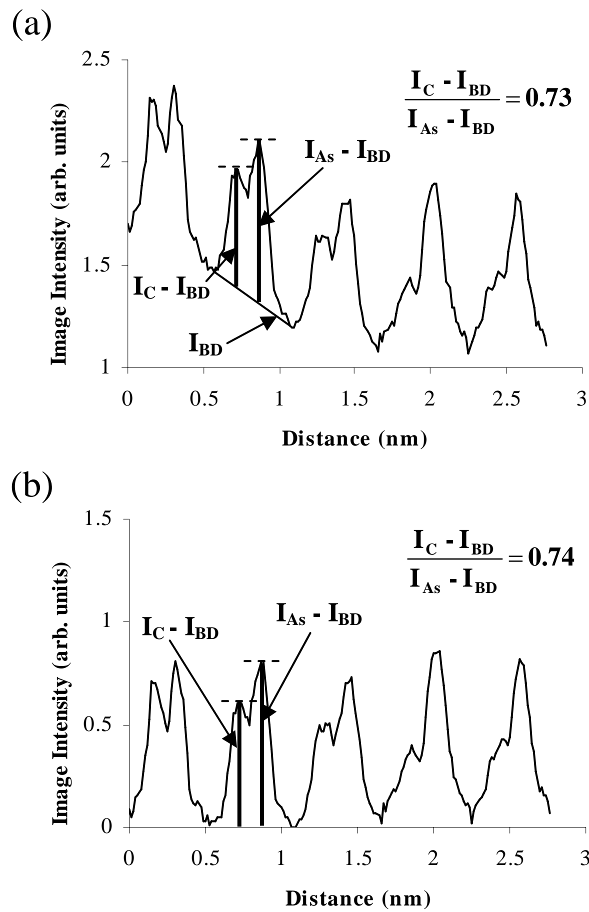

Fig. 4. (a) HAADF intensity profile drawn across a GaAs / AlAs interface in the superlattice. (b) The background-removed version of the intensity profile shown in (a). Every point of the intensity profiles was generated from the average of 10 pixels summed along the $[1\bar{1}0]$ direction. Note that the value of the dumbbell column ratio is also given in each case. The column ratio is in close agreement in the profiles.

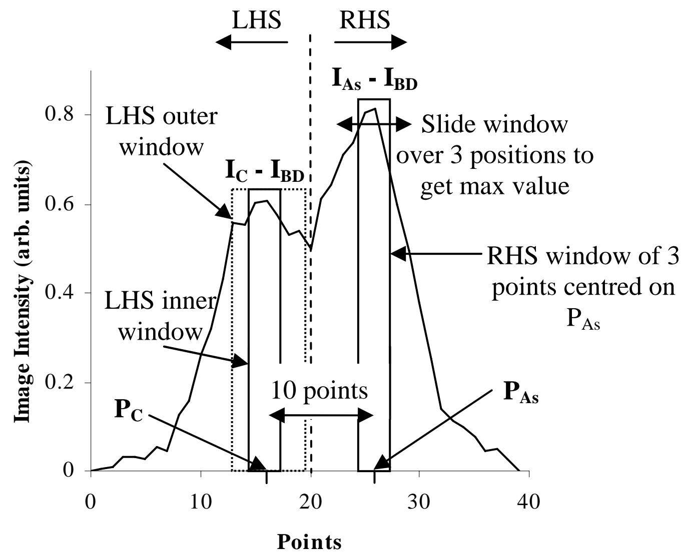

Fig. 5. An example of a single 40 point background-removed HAADF intensity profile along the [001] direction. Every point of the intensity profile was generated from the average of 10 background-removed image pixels summed along the $[1\bar{1}0]$ direction. See text for explanation.

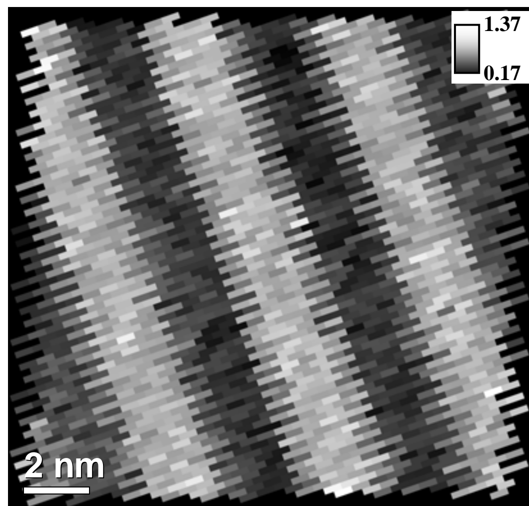

Fig. 6. The column ratio map of Fig. 2(d) re-plotted with the spaces between dumbbells filled in along the [001] direction.

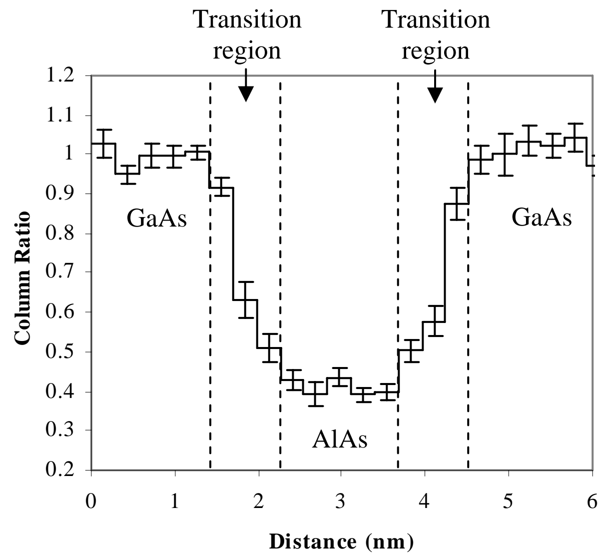

Fig. 7. An average column ratio profile taken across the column ratio map of the superlattice. Every point of the profile was generated from the average of 10 dumbbells summed along the $[1\bar{1}0]$ direction. The profile reveals the presence of 3ML wide transition regions across each interface.

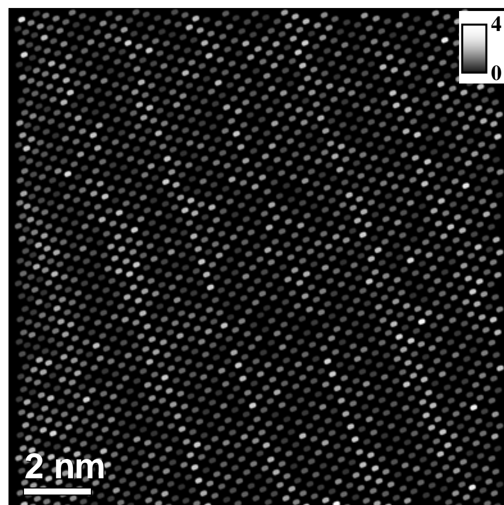

Fig. 8. The column ratio map of Fig. 2(d) re-plotted as a standard deviation departure map. Each dumbbell has a value that denotes how many standard deviations away from the mean its column ratio value is.

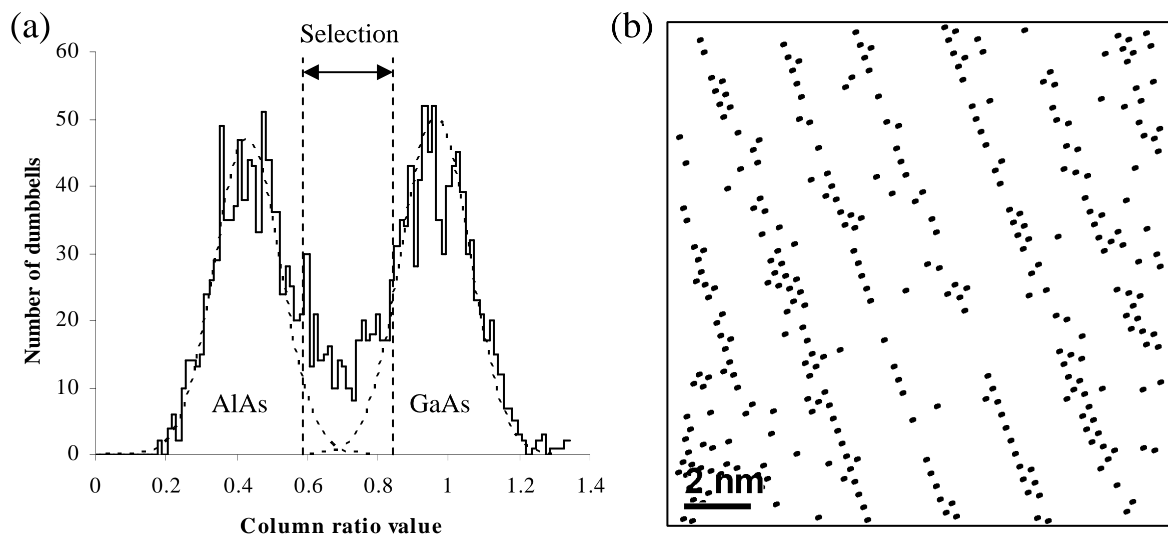

Fig. 9. (a) A histogram of the column ratio value calculated from the column ratio map in Fig. 2(d). Two visible peaks correspond to AlAs-like and GaAs-like dumbbells. Two Gaussian peaks associated with the mean and standard deviation values of AlAs and GaAs are also shown (dotted lines). (b) The column ratio map of Fig. 2(d) re-plotted to highlight the positions of the dumbbells that have values within the range given by the selection in (a).

Acknowledgements

This work was funded by the Engineering and Physical Sciences Research Council. We are grateful to Martin Holland for growing the MBE materials and to Brian Miller for specimen preparation. We would also like to thank Andrew Bleloch, Mhairi Gass, Uwe Falke and Meiken Falke for SuperSTEM technical support and advice.

Reference

[1] M. Haider, H. Rose, S. Uhlemann, E. Schwan, B. Kabius, K. Urban, Ultramicroscopy 75 (1998) 53-60

[2] P. E. Batson, Ultramicroscopy 96 (2003) 239-249

[3] N. Dellby, O L. Krivanek, P. D. Nellist, P. E. Batson, A. R. Lupini, Journal of Microscopy 50(3) (2001) 177-185

[4] M. Valera, A. R. Lupini, K. van Benthem, A. Y. Borisevich, M. F. Chisholm, N. Shibata, E. Abe, S. J. Pennycook, Annual Review of Materials Research, Vol. 35 (2005) 359-569

[5] O. L. Krivanek, N. Dellby, A. R. Lupini, Ultramicroscopy 78 (1999) 1-11

[6] O. L. Krivanek, P. D. Nellist, N. Dellby, M. F. Murfitt, Z. Szilagyi, Ultramicroscopy 96 (2003) 229-237

[7] J. H. Davies, The physics of low-dimensional semiconductors, Cambridge University Press (2005)

[8] S. J. Pennycook, D. E. Jesson, Physical Review Letters, Volume 64 (1990) Number 6

[9] S. J. Pennycook, D. E. Jesson, Ultramicroscopy 37 (1991) 14

[10] S. J. Pennycook, B. Rafferty, P. D. Nellist, Microscopy Microanalysis 6 (2000) 343-352

[11] B. Rafferty, P. Nellist, J. Pennycook, Journal of Electron Microscopy 50 (2001) 227-233

[12] P. D. Nellist, S. J. Pennycook, Scanning Microscopy Vol. 11 (1997) 81-90

[13] N. Ikarashi, K. Ishida, Journal of Materials Science: Materials in Electronics 7 (1996) 285-295

[14] H. Larkner, B. Bollig, S. Ungerechts, E. Kubalek, Journal of Physics D: Applied Physics 29 (1996) 1767-1778

[15] W. Neumann, Materials Chemistry and Physics 81 (2003) 364-367

[16] R. F. Loane, P. Xu, J. Silcox, Ultramicroscopy 40 (1992) 121-138

[17] K. Y. Cheng, Proceedings of the IEEE, Vol. 85 (1997) No. 11

[18] D. O. Klenov, S. Stemmer, Ultramicroscopy 106 (2006) 889-901

[19] M. M. J. Treacy, Ultramicroscopy 52 (1993) 31-53

[20] T. Plamann, M. J. Hytch, Ultramicroscopy 78 (1999) 153-161

[21] S. Hillyard, R. F. Loane, J. Silcox, Ultramicroscopy 49 (1993) 14-25

[22] J. M. Cowley, Y. Huang, Ultramicroscopy 40 (1992) 171-180

[23] S. Hillyard, J. Silcox, Ultramicroscopy 58 (1995) 6-17

[24] C. Dwyer, J. Etheridge, Ultramicroscopy 96 (2003) 343-360

[25] C. P. Scott, A. J. Craven, P. Hatto, C. Davies, Journal of Microscopy, Vol. 182 Pt 3 (1996) pp. 186-191

[26] B. R. Nag, Semiconductor Science Technology 19 (2004) 162-166

[27] R. A. Stradling, P. C. Klipstein, Growth and characterisation of semiconductors, Adam Hilger (1991)

[28] Y-M Kim, J-M Jeong, J-G Kim, Y-J Kim, Journal of Korean Physical Society, Vol. 48 No. 2 (2006) pp. 250-255

[29] P. L. Galindo, S. Kret, A. M. Sanchez, J-Y Laval, A. Yanez, J. Pizarro, E. Guerrero, T. Ben, S. I. Molina, Ultramicroscopy 107 (2007) 1186-1193